ARL-TR-8851 ● Nov 2019

DEVCOM ARMY RESEARCH LABORATORY

Additive Manufacturing Utilizing a Novel In-Line Mixing System for Design of Functionally Graded Ceramic Composites

by Joshua Pelz, Nicholas Ku, Marc Meyers, and Lionel Vargas-Gonzalez

NOTICES

Disclaimers

The findings in this report are not to be construed as an official Department of the Army position unless so designated by other authorized documents.

Citation of manufacturer's or trade names does not constitute an official endorsement or approval of the use thereof.

Destroy this report when it is no longer needed. Do not return it to the originator.

ARL-TR-8851 ● Nov 2019

Additive Manufacturing Utilizing a Novel In-Line Mixing System for Design of Functionally Graded Ceramic Composites

Nicholas Ku and Lionel Vargas-Gonzalez
Weapons and Materials Research Directorate, CCDC Army Research Laboratory

Joshua Pelz and Marc Meyers
University of California, San Diego

REPORT DOCUMENTATION PAGE

Form Approved
OMB No. 0704-0188

1. REPORT DATE *(DD-MM-YYYY)*	2. REPORT TYPE	3. DATES COVERED (From - To)
November 2019	Technical Report	July 2018–September 2019

4. TITLE AND SUBTITLE
Additive Manufacturing Utilizing a Novel In-Line Mixing System for Design of Functionally Graded Ceramic Composites

5a. CONTRACT NUMBER

5b. GRANT NUMBER

5c. PROGRAM ELEMENT NUMBER

6. AUTHOR(S)
Joshua Pelz, Nicholas Ku, Marc Meyers, and Lionel Vargas-Gonzalez

5d. PROJECT NUMBER

5e. TASK NUMBER

5f. WORK UNIT NUMBER

7. PERFORMING ORGANIZATION NAME(S) AND ADDRESS(ES)
CCDC Army Research Laboratory
ATTN: FCDD-RLW-ME
Aberdeen Proving Ground, MD 21005

8. PERFORMING ORGANIZATION REPORT NUMBER
ARL-TR-8851

9. SPONSORING/MONITORING AGENCY NAME(S) AND ADDRESS(ES)

10. SPONSOR/MONITOR'S ACRONYM(S)

11. SPONSOR/MONITOR'S REPORT NUMBER(S)

12. DISTRIBUTION/AVAILABILITY STATEMENT
Approved for public release; distribution is unlimited.

13. SUPPLEMENTARY NOTES
ORCID ID(s): Nicholas Ku, 0000-0002-1276-4927; Lionel Vargas-Gonzalez, 0000-0001-6500-1686

14. ABSTRACT
Additive manufacturing is being explored as a processing technique to research and develop functionally graded ceramic composites. This report highlights the development of a direct ink writing system with multimaterial and in-line mixing capabilities for printing inks composed of high solids-loaded ceramic particulate suspensions. The custom direct ink writing system has two primary components, the print head and the feed system, and interfaces with a low-cost fused-deposition modeling 3-D printer. The feed system inputs ceramic ink to the print head at a specified composition. The print head uses an auger to mix and extrude multiple inks through a single nozzle. Precise conveyance is achieved via the auger, resulting in an improved start/stop response over syringe-based direct ink writing systems. Additionally, in-line mixing uniquely enables the formation of composition gradients. Silicon carbide and boron carbide composites were successfully printed with layered and gradient structures.

15. SUBJECT TERMS
ceramic processing, ceramic slurry rheology, additive manufacturing, functionally graded materials, ceramic rapid prototyping

16. SECURITY CLASSIFICATION OF:			17. LIMITATION OF ABSTRACT	18. NUMBER OF PAGES	19a. NAME OF RESPONSIBLE PERSON
a. REPORT	b. ABSTRACT	c. THIS PAGE			Nicholas Ku
Unclassified	Unclassified	Unclassified	UU	33	19b. TELEPHONE NUMBER (Include area code) (410) 306-4592

Contents

List of Figures

Acknowledgments

This research was sponsored by the US Army Combat Capabilities Development Command Army Research Laboratory and was accomplished under Cooperative Agreement Number W911NF-19-2-0054. The views and conclusions contained in this document are those of the authors and should not be interpreted as representing the official policies, either expressed or implied, of the Army Research Laboratory or the US Government. The US Government is authorized to reproduce and distribute reprints for Government purposes notwithstanding any copyright notation herein.

1. Introduction

The impetus for advancing brittle ceramic materials used for armor applications has been identified as both an increased mass efficiency for greater weight reduction and enhanced performance against ballistic threats through manipulating the physics of failure. Development of functionally graded ceramic composites is a potential solution for enabling new dynamic fracture and deformation mechanisms in armor materials, surpassing that of the individual intrinsic material behaviors. However, engineering of these composite structures is currently limited due to the stochastic nature of traditional powder mixing and processing. Thus, additive manufacturing (AM) is being studied as an enabling technology for processing discrete mesostructural features, complex geometries, and compositional variation.

Various traditional ceramic forming technologies exist including pressing, extrusion, slip casting, tape casting, and injection molding. However, these traditional forming techniques often only allow 2-D design freedom, cannot create internal or multiscaled features, and require complicated and expensive dies.[1] On the other hand, AM enables the production of parts with complex, multiscaled geometries including internal structures. Additionally, multimaterial AM allows for the mimicking of biological composites that take advantage of hierarchical structures and compositional gradients to increase their strength and toughness.[2–4] Three main categories of AM exist: extrusion-based processes, liquid-bed processes, and powder-bed processes. Extrusion-based processes, such as fused deposition modeling (FDM) and direct ink writing (DIW), raster a print head across the print-bed layer by layer while extruding a continuous trace of material. Liquid-bed processes, such as stereolithography, use a laser or other energy source to cure resin layer-by-layer as the build plate further submerges. Powder-bed processes, such as selective laser melting/sintering, use a laser or other high-power energy source to melt/sinter powder in a layer-by-layer fashion as the print-bed moves downward and more powder is spread over the print area.

Exploration of next-generation ceramic armor composites will require high-resolution, multimaterial, and mixing capabilities to print structures that have compositional gradients, internal structures, and hierarchical organization. Powder- and liquid-bed processes run into issues with multimaterial applications because the powder/liquid vat must be switched for every composition variation. The extrusion-based FDM method of ceramic-filled polymer filament creates parts with low green density, leading to low percent theoretical density following sintering. Ink jetting, a popular commercial solution to ceramic AM, again produces porous parts with low density. DIW, on the other hand, shows significant promise for studying these composites because it fulfills each requirement.

The DIW technique, also known as robocasting, involves extrusion of a line of highly loaded colloidal suspension, termed "ink", through a small nozzle in a specific pattern layer by layer to produce a 3-D part.[5] Unlike FDM, where printed material solidifies directly after extrusion, DIW relies on the yield-pseudoplastic rheological behavior of the ink for structural integrity following extrusion. Yield-pseudoplastic rheology gives the ink structural integrity up to its yield stress, followed by shear-thinning behavior.[6] When the ink is designed with this rheological behavior, it can easily flow through the nozzle due to the high-shear environment, but after extrusion (yield stress goes to zero) it can retain its shape due to its yield strength. Equally as important as ink printability, is postprint processing performance; namely shape retention and densification characteristics. A postprocessed part must be as close to 100% theoretical density as possible to have acceptable ballistic performance.[7–9] A prerequisite of high sintered density is high green density, necessitating high particulate-loading and low binder/dispersant content in the ink.[10] However, high solids-loading and low binder/dispersant content leads to dilatant behavior and poor printability. Thus, a balance must be found between printability, yield-point, and postprint processing behavior. These competing factors result in a complex ink design process, where constituent type, content, and interaction are of paramount importance. Although complicated, understanding of colloidal ink processing has advanced to a point where there is flexibility available in terms of binder/dispersant selection, allowing selection of a variety of material systems.[6]

2. Methods

2.1 Design Overview

The custom DIW system has two main modules, the print head and the feed system. These modules were designed and optimized, using Autodesk's computer-aided design (CAD) software Fusion 360, to allow simultaneous extrusion of multiple ceramic inks through a single nozzle. The feed system has two units that are controlled independently, allowing output of material A, B, or any combination of the two. The ink is fed, using leadscrew driven plungers, through tubes to the print head. The print head contains an auger that achieves in-line mixing and volumetric extrusion, enabling simultaneous extrusion of inks with different rheological properties. The print head is designed to integrate with a LulzBot Taz 6 3-D printer, which removes the need for development of a 3-axis CNC and G-code communication protocols. The Taz 6 was chosen due to suitable precision, print volume, and open-source design. In order to integrate the print head, the Taz 6 firmware was modified to account for temperature-related errors, print head spatial

variations, and custom tool path modifications. The print head is made from plastic parts, which were printed using the Taz 6 with its provided FDM print head. Communication between the Taz 6, which controls the print head, and the feed system is accomplished with the I2C communication protocol. The I2C protocol allows single character transmission from the Taz 6 to the feed system microcontroller. As each G-code line is processed by the Taz 6, it is echoed character by character to the feed system. The feed system microcontroller then parses each G-code line and extracts values for extrusion lengths, feed rates, and ratios. This line-by-line communication is a robust method to precisely sync the material output from the feed system with the movements of the print head. Additionally, G-code files can be easily modified in any text editor to include additional information that could benefit the DIW process.

2.2 Print Head

The print head uses its auger to actively mix and extrude ceramic ink received from the feed system. The auger has three sections, with each performing a distinct function to successfully mix and convey material from the feed inlets through the nozzle. The first section has deep channels at a large pitch, which enables a large flow rate and small residence time. The second section has kneading blocks offset by 60° and works to provide additional shearing action. A 60° offset between adjacent kneading blocks provides a small amount of conveying action in combination with good mixing action. The third section has shallow channels at a small pitch, which provides a large conveying force and high residence time. The last section develops the necessary pressure to extrude material through a small nozzle orifice. The print head interfaces with the Taz 6 via the T-adapter with communication handled through the Taz 6 wiring harness. The Taz 6 controls the print head's 3-D positioning and auger speed. Figure 1 shows CAD renderings and cross-section analyses developed in Fusion 360.

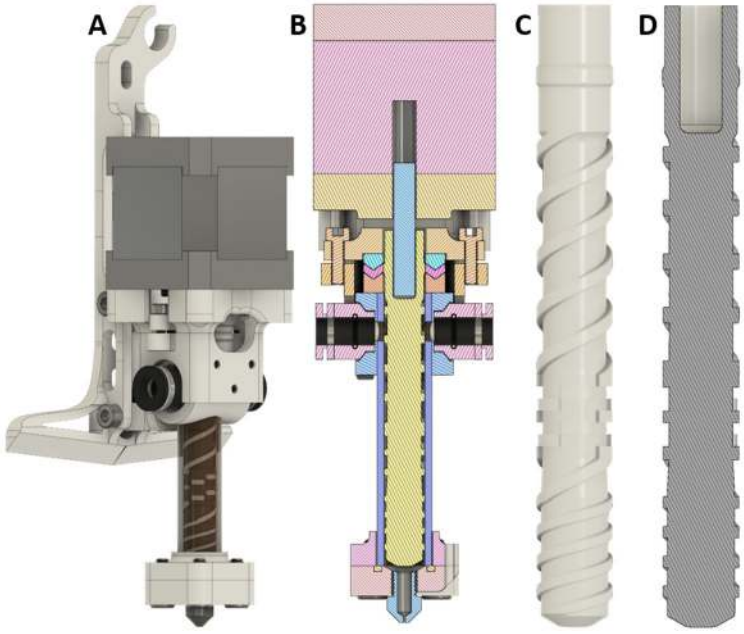

Fig. 1 The print head was designed and rendered in Fusion 360. a) Rendering and b) cross section of the full print head assembly, and c) rendering and d) cross section of the auger.

The majority of the print head's components are printed using the Taz 6's provided FDM tool head. The auger is printed out of a polycarbonate-acrylonitrile butadiene styrene (ABS) alloy, which has improved strength and wear resistance over conventional ABS filament. Other printed components, which do not come in contact with the ceramic ink, are made out of ABS. The print head can be easily disassembled to clean or replace components. Figure 2 shows an exploded view of the print head with each component labeled.

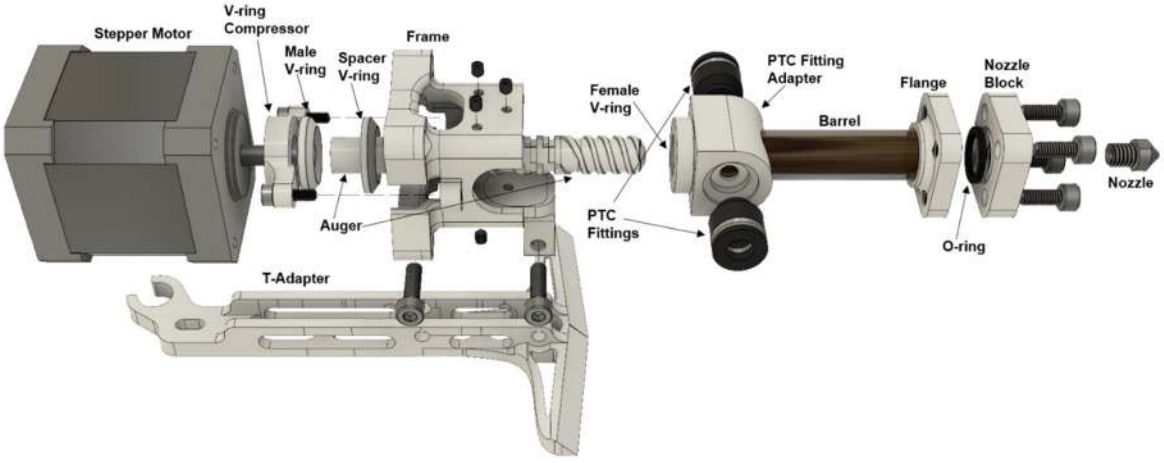

Fig. 2 Exploded view of the print head to demonstrate component positioning

The V-ring assembly provides a rotary seal between the top of the barrel and the auger. The spacer V-ring is press fit around the extruded section of the auger. Proper sealing force is maintained with the V-ring compressor, which is adjusted using two M3 bolts. Two push-to-connect (PTC) fittings are used to attach the feed tubes. The barrel, a 3/8-inch inner diameter polycarbonate tube, has two holes aligned with the PTC fittings. The PTC fitting adapter and flange are press fit around the barrel. The PTC fitting adapter slides into the bottom of the frame and is secured in place with six cone-point M3 setscrews. The stepper motor is bolted to the frame with its D-cut shaft aligned in the female end of the auger. A square-profile O-ring seals the flange to the nozzle block, which is tapped with an M6 thread for compatibility with any standard FDM 3-D printer nozzle. This allows the user to tune nozzle orifice size to their specific application. A variety of abrasion-resistant 3-D printer nozzles exist, which are necessary for the highly abrasive ceramic inks.

2.3 Feed System

The feed system includes two identical units, which are independently controlled to allow input of material A, B, or any ratio of the two to the print head. The use of feed system units provides a scalable design, which could be modified to support additional materials by simply adding more units. Each unit has a syringe (ink reservoir) with a capacity of 100 mL. Figure 3 displays a feed system unit, designed and rendered in Fusion 360. The syringe can be removed, loaded with ceramic ink, and slid back into position. A short length of 16 AWG wire can be used to break the plunger gasket seal to allow it to slide into contact with the loaded ink. If the plunger does not contact the ink, the compressible air gap will significantly reduce feed rate control. Figure 4 shows an exploded view of the feed system unit with labeled components.

Fig. 3 The feed system was designed and rendered in Fusion 360. This feed system unit has a capacity of 100 mL, provides excellent positional precision using a geared down leadscrew, and can generate pressures over 100 psi.

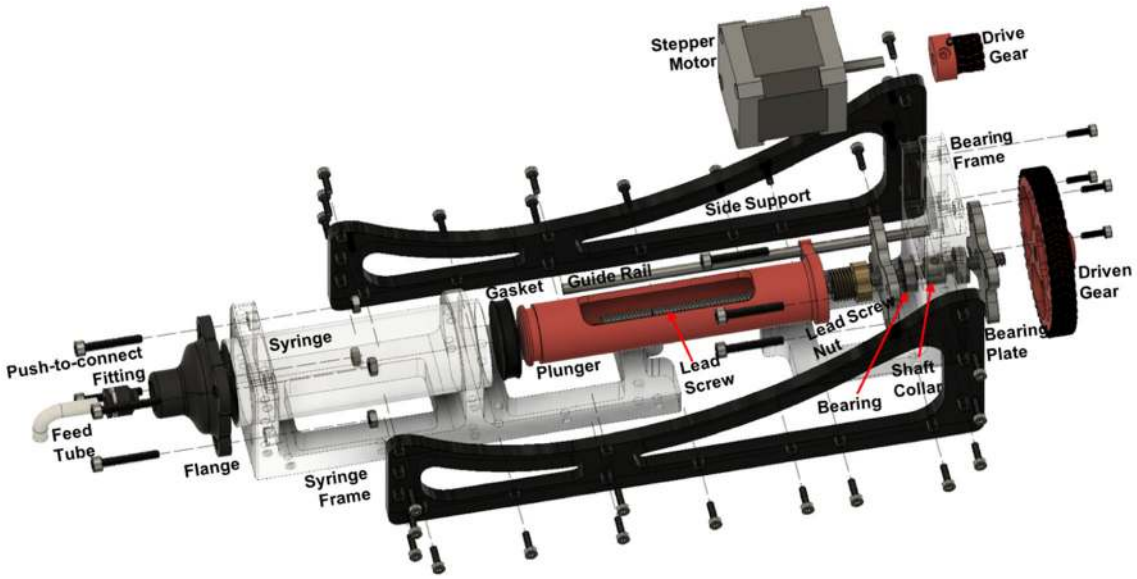

Fig. 4 Exploded view of the feed system showing component positioning

Each feed system unit consists of a stepper motor, bearing assembly, drive and driven gear, leadscrew, leadscrew nut, guide rail, plunger and gasket, modified syringe, flange, push-to-connect fitting, two side supports, bearing frame, and syringe frame. The bearing assembly includes two bearings, two bearing plates, and a shaft collar. The bearing assembly reduces rotational resistance while locking the leadscrew's linear position. The collar is fastened onto the leadscrew, leaving 30 mm exposed on the shorter side. The bearings are slid on either side of the collar

and then inserted into the appropriate hole in the bearing frame. The bearing plates are then fastened on either side using 25-mm-long 4M bolts. The driven gear is attached to the end of the leadscrew and secured with two 3M cup-point setscrews. The drive gear is attached to the stepper motor using a 3M cup-point setscrew and the stepper motor is bolted onto the bearing frame with the drive gear teeth correctly aligned to the driven gear. The leadscrew nut is glued into place in the plunger and threaded onto the leadscrew. The guide rail, a 5-mm-diameter steel rod, is slid through the plunger arm and glued in place to the bearing frame and syringe frame. The plunger gasket was taken off the original plunger and fitted over the printed plunger head. The side supports can then be secured to the bearing and syringe frames using 4M bolts. The modified syringe is glued in place inside the flange, which bolts to the syringe frame. A PTC fitting, glued into the flange, provides a robust connection with the feed tube and prevents material leakage. Figure 5 shows a cross-section analysis of a feed system unit, which highlights the mechanics of the drivetrain and positioning of components. The drivetrain, which includes a drive gear, driven gear, and leadscrew, converts the rotational motion of the stepper motor into the plunger's linear motion. The gearing ratio is 9:47, which gives a torque multiplication factor of 5.22. The leadscrew has a lead of 1/16 inch per revolution, which, in combination with the gearing ratio, results in very precise linear movements of less than 0.01 mm per stepper motor step. Figure 6 highlights various subassemblies including the gears, guide rail, and bearing assembly. Custom feed system parts were printed in ABS.

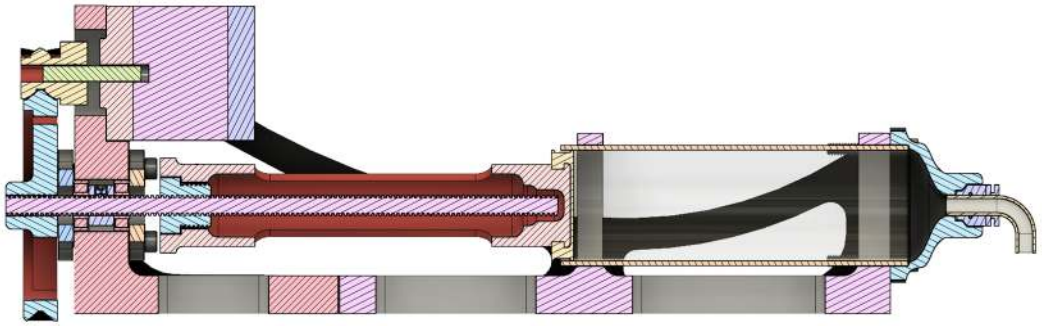

Fig. 5 Feed system unit cross section highlighting the mechanics of its drivetrain, which includes a drive gear, driven gear, and precision leadscrew. The drivetrain creates a large mechanical advantage and enables very small linear movements, below 0.01 mm per stepper motor step.

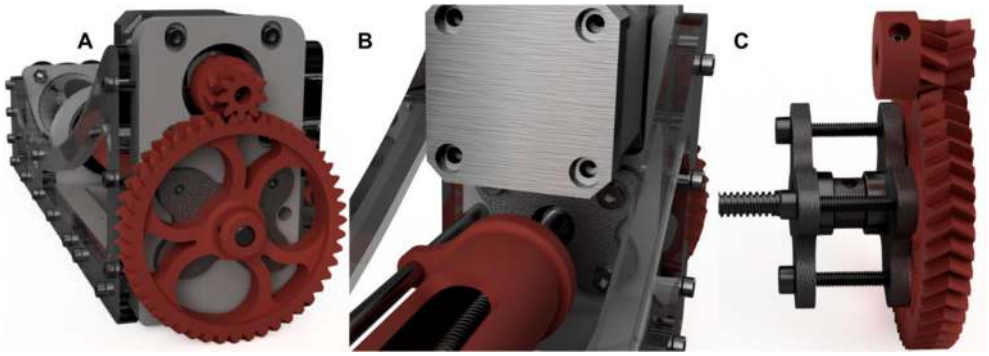

Fig. 6 Renderings of a feed system unit highlighting various subassemblies. a) A 9:47 gearing ratio is used to couple the stepper motor with the leadscrew. b) The plunger uses a guide-rail to prevent rotation. c) The bearing assembly includes a shaft collar, two bearings, and two bearing plates. This robust setup locks the linear position of the leadscrew and reduces rotational resistance.

Several feed system parts were validated using finite element analysis simulations. Simulation studies were performed in Fusion 360 with an applied pressure of 100 psi at the plunger gasket, to simulate maximum operating conditions. ABS plastic was used as the simulation material. Compared with cast or extruded parts, 3-D printed parts have reduced strength and anisotropic mechanical properties due to weaker interfaces between layers. Therefore, a minimum factor of safety of 2.5 was chosen to validate these parts. In order to reduce print time and material use, topology optimization studies were paired with finite element analysis static stress studies for the side supports and plunger arm. Simulation criteria included a target mass reduction of 40% and the objective of maximizing stiffness. Boundaries were placed at each end to preserve necessary geometries. Topology optimization results were used to inform the removal of non-essential material from initial designs. Modified designs were then run through secondary finite element analysis simulations at 100 psi to verify their structural integrity. Figure 7 showcases results for the plunger, where mass reduction through shape optimization reduced printing time and material use by nearly 30%.

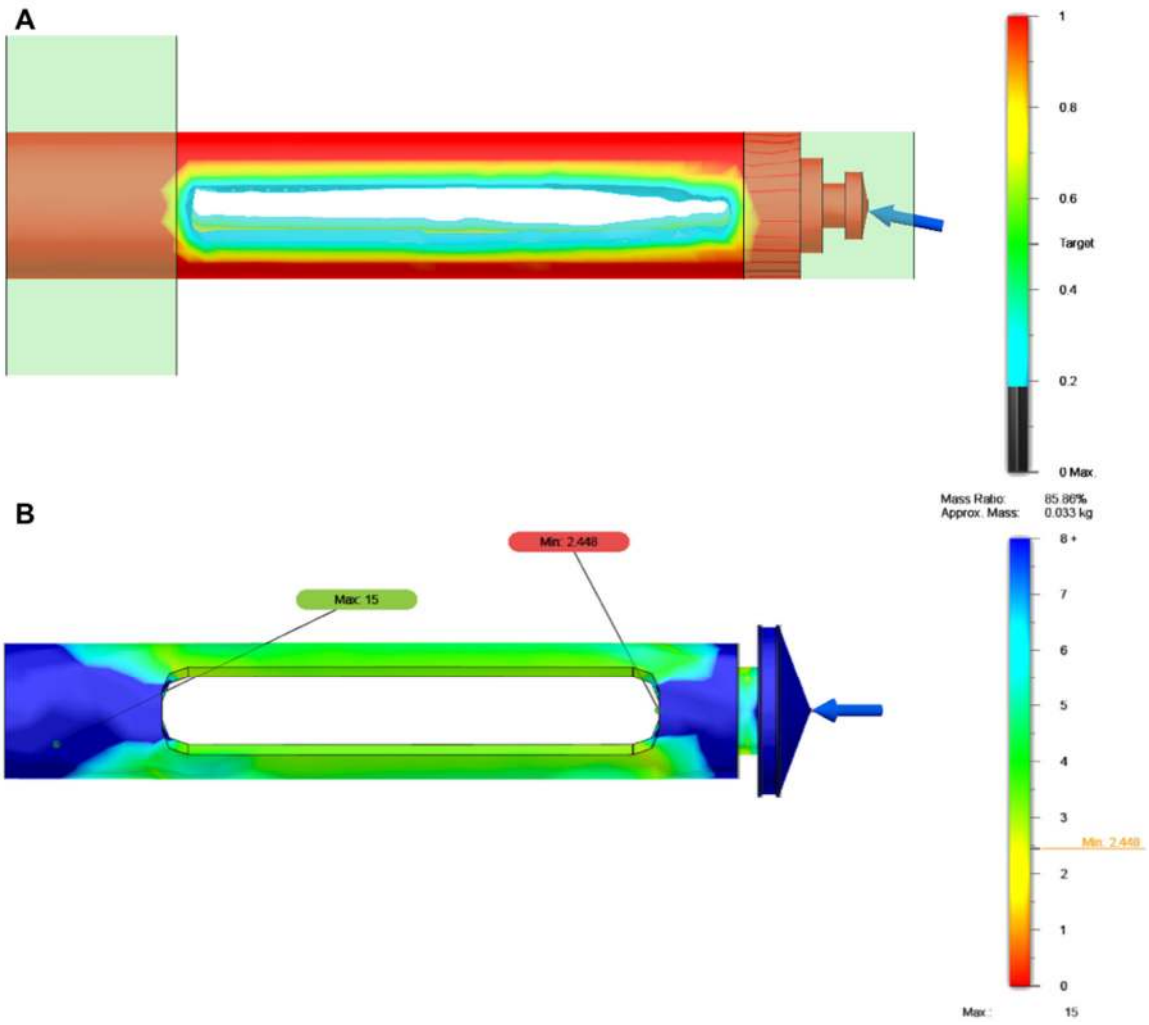

Fig. 7 CAD simulation studies were performed in Fusion 360 with an applied pressure of 100 psi. a) Topology optimization was used to remove non-essential material. b) The shape optimized plunger, designed out of ABS plastic, was studied using a static-stress simulation to validate the topology optimization solution.

Vector data files for the feed system side supports and bearing plates, which were exported from Fusion 360 and edited in Autodesk's CAD software AutoCAD, are shown in Fig. 8. First-generation bearing plates were made from 1/4-inch-thick aluminum plate, but during feed system operation significant bending caused plastic deformation and loss of feed precision. Therefore, the bearing plates were water-jet cut out of 3/16-inch-thick steel plate. Side supports were laser cut out of 1/4-inch acrylic. Each feed system unit has a front and rear bearing plate. The rear bearing plate has smaller holes, which are tapped with 4M threads. Threading directly into the rear plate allows the driven gear to sit flush against it, instead of needing space for a nut.

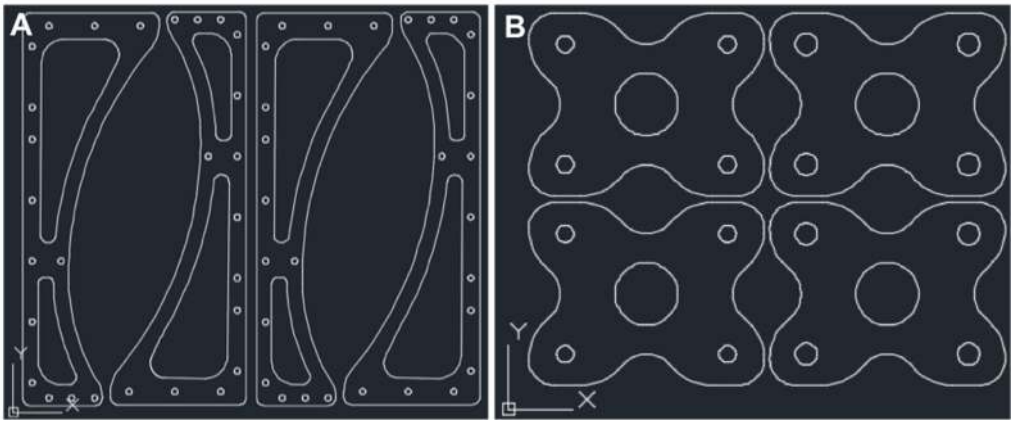

Fig. 8 Vector data files for two feed system units: a) Side supports machined with a laser cutter and b) bearing plates machined with a water-jet cutter

2.4 Control Structure

While DIW a ceramic part, the Taz 6 and feed system must communicate so the material feed matches the print head motion and extrusion. The Taz 6 follows a G-code file to control the print head auger's rotation direction and speed as well as the print head's x, y, and z position. The feed system, controlled by a separate Arduino Mega microcontroller, relies on echoed G-code lines to determine feed rate, volume, and ratio. The diagram in Fig. 9 shows the structure of the feed system control hardware. The feed system controller consists of an Arduino Mega, two Big Easy Drivers (BEDs), an Arduino power supply, and two BED power supplies.

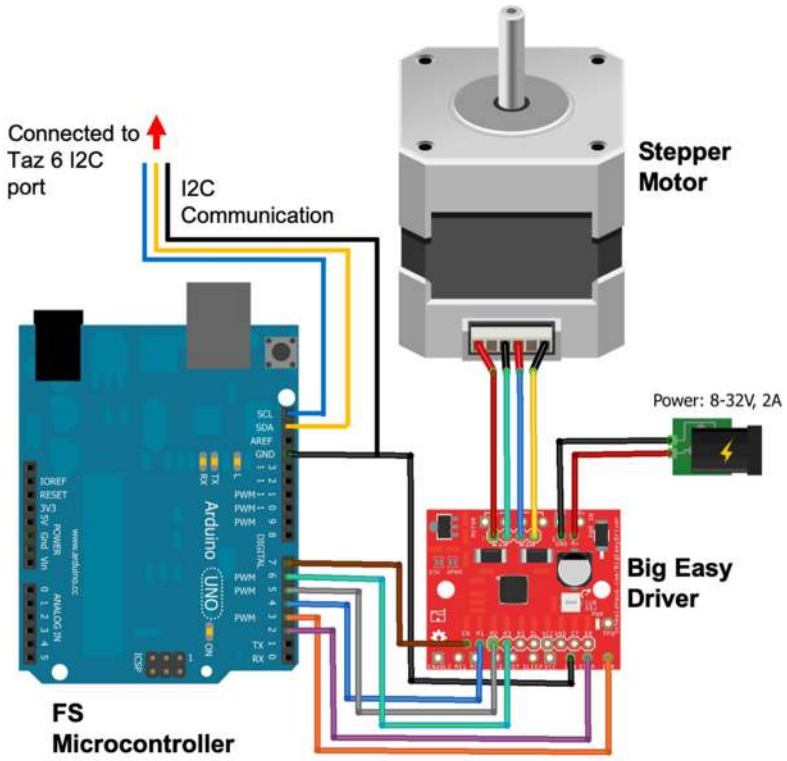

Fig. 9 Wiring schematic showing connections between the feed system controller components

An Arduino program was written to parse the echoed G-code lines and control the stepper motors to keep the print head and feed system synchronized. When the Taz 6 reads a G-code command off its secure digital (SD) card, the G-code line is sent character by character to the feed system microcontroller using the I2C protocol. The G-code line is then stored in an array and searched for "F", "E", and "R" qualifiers. An F designates feed rate in millimeters per minute, an E designates extrusion length in millimeters, and an R designates the ratio between 0 to 1, where 0 is 100% material A and 1 is 100% material B. If any of these qualifiers are found, the values are stored, and flags are set for each respective qualifier. This function is blocking and will interrupt the main loop each time a new line of G-code is received.

The main loop has three sections, the serial monitor check, the flag check, and the step timing. The first section checks the serial monitor for user input, either an "e" or "r", and if present executes the respective functions. If the user inputs an e, both stepper motors will turn forward one revolution. If the user inputs an r, both stepper motors will turn backward one revolution. These functions allow the user to increase or decrease pressure to the print head. The second section checks for flags signifying a new extrusion length or ratio has been received. If a new extrusion length is flagged available, the extrusion sign is checked to set step direction and

the feed function is called. The feed function updates the steps stepper motor A and B must take based on new extrusion length and current ratio. The function also checks for the new rate flag, and, if available, updates the stepping period. If a new ratio is flagged available, the ratio is checked and depending on the value several actions will proceed. Case 1 (ratio equals 0): stepper motor A is primed, stepper motor B is reversed, and then stepper motor B is disabled to reduce idle time. Case 2 (ratio equals 1): stepper motor B is primed, stepper motor A is reversed, and then stepper motor A is disabled to reduce idle time. Case 3 (ratio is between 0 and 1): both stepper motors are enabled, the motor that was previously stepping will be half-reversed, and the stepper motor that was previously disabled will be half-primed. Case 4 (ratio equals –1): both stepper motors are disabled. The third section checks to see if either stepper motor needs to step. If a step needs to be taken, the time since it last stepped is compared to the stepping period and, if greater, a single step is executed. The feed system motors are operated in microstepping mode to reduce vibration and increase feed precision.

The extrusion length calculated by the Taz 6 must be converted into an extrusion volume and then into linear distances each feed system unit plunger must move. The gearing ratio and leadscrew threads-per-inch values relate the rotation of the drive gear to the linear motion of the plunger. The travel per revolution is calculated using Eq. 1.

$$x_{travel\frac{mm}{rev}} = \frac{9}{47} * \frac{1}{16} * \frac{25.4\ mm}{1\ in}\,. \tag{1}$$

The gearing ratio is 9:47 and the leadscrew's threads-per-inch is 1/16. Breaking the drive gear's revolution into steps allows x_{travel} to be converted from per revolution to per step (Eq. 2).

$$x_{travel\frac{mm}{microstep}} = \frac{9}{47} * \frac{1}{16} * \frac{25.4\ mm}{1\ in} * \frac{1}{3200}\,. \tag{2}$$

The stepper motors are operated in sixteenth-step mode, resulting in 3200 microsteps per revolution. The feed system feed volume per microstep rate is calculated using the known feed system syringe diameter and is related to the G-code extrusion length with Eq. 3. The resulting stepping factor is the number of microsteps needed to equal a G-code extrusion length of 1 mm.

$$stepping\ factor = \frac{x_{travel\frac{mm}{microstep}} * \pi * (\frac{D_S}{2})^2}{1mm * \pi * \left(\frac{D_F}{2}\right)^2}\,. \tag{3}$$

If the syringe diameter (D_S) is 35 mm and the filament diameter (D_F) is 3 mm, the stepping factor is calculated as 92.52. Next, using the ratio, the number of steps each stepper motor must take can be updated.

$$Steps_A = E * 92.52 * (1 - R) \quad (4)$$

$$Steps_B = E * 92.52 * (R) \quad (5)$$

The G-code extrusion length, E, is converted into a number of microsteps for stepper motors A and B using Eqs. 4 and 5.

2.5 LulzBot Taz 6 Integration

The LulzBot Taz 6 3-D printer is the latest version of Aleph Objects successful line of desktop FDM printers. Key features include a large print volume, robust and precise performance, and an open-source, modular design. When developing this custom DIW system, the open-source, modular design was extremely important because it supported modification of the firmware and hardware. In fact, many of the Taz 6's parts are printed using Aleph Object's arsenal of 3-D printers, which makes modifications and repairs more accessible.

To swap the provided FDM tool head out with the DIW print head, the wiring harness connector is detached and a single M3 bolt is unscrewed. The DIW print head wiring connector can then be plugged into the Taz 6 wiring harness and M3 bolt screwed back in once the print head T-adapter is aligned in the Taz 6 tool head adapter's V-channel. Shorter feed tubes reduce the pressure gradients that develop in the ink during operation, so the feed system units are mounted onto the top of the Taz 6 frame with their outlets positioned above the middle of the print bed. To reduce wire length, the control structure hardware is also mounted on top of the LulzBot Taz 6 frame. The print bed is borosilicate glass covered with a thin PEI, or polyethylenimine, sheet and can be heated.

Following hardware integration, the firmware must be modified to account for several differences between the provided FDM head and custom DIW print head. To modify the firmware, the */Software/Marlin version 1.x.x.x* zip file was downloaded from www.lulzbot.com. The firmware was modified using the Arduino Integrated Development Environment. Several sections of the firmware file were modified starting with the Conditionals_LulzBot.h tab:

1. Change '#define LULZBOT_EXTRUDE_MINTEMP' from 120 to 5.
2. Change '#define LULZBOT_INVERT_E0_DIR' from true to false.
3. Change '#define LULZBOT_INVERT_E1_DIR' from true to false.

4. Change ‘#define LULZBOT_Z_SAFE_HOMING_Y_POINT’ from 258 to 254.
5. Change ‘#define LULZBOT_MANUAL_FEEDRATE_E from 1.0 to 2.0.
6. For ‘#elif defined(LULZBOT_USE_AUTOLEVELING) && defined(LULZBOT_TAZ_BED)’
    - Change ‘LULZBOT_RIGHT_PROBE_BED_POSITION’ from 288 to 286.
    - Change ‘LULZBOT_BACK_PROBE_BED_POSITION’ from 289 to 285.
7. Change LULZBOT_NOZZLE_PARK_POINT {x, y, z} to { 206, 236, 3 }.
8. For the #define LULZBOT_ACTION_ON_PAUSE_AND_RESUME find the #elif for LULZBOT_IS_TAZ. Change the code to: “G91\nG0 Z15 F600\nG90\nG0 X206 Y236 F3000\nG0 Z3 F600\nM117 Print aborted.”

Next, Configuration.h was edited:

1. Change ‘#define TEMP_SENSOR_0’ from LULZBOT_TEMP_SENSOR_0 to 998.
2. Add ‘//’ in front of ‘#define USE_XMAX_PLUG LULZBOT_USE_XMAX_PLUG’ to comment it out.

Next, Configuration_LulzBot.h was edited:

1. Delete // in front of ‘#define LULZBOT_Oliveoil_TAZ6’.
2. Delete // in front of ‘#define TOOLHEAD_Tilapia_SingleExtruder’.

Next, Marlin_main.cpp was edited:

1. Search for 'void process_next_command()’. Inside this function on the line before the comment “// Parse the next command in the queue” paste the following code:

    Wire.beginTransmission(125);

    Wire.write(current_command);

    Wire.endTransmission();

    This code will make the Taz 6 echo each line of G-code to the feed system Arduino Mega right as it processes that line of G-code.

2.6 G-code Generation

In order to simplify the printing process, Slic3r, free slicing software commonly used for FDM printers, is used to generate G-code. Several Slic3r profile modifications must be made in order for the print head to be compatible with the G-code, which is usually generated for an FDM toolhead.

1. Due to the fluid dynamics of the ink and attainable pressure of the DIW system, a lower print speed of 4 mm/s was used for testing.

2. Print head heating is not supported, so extruder temperature must be set to 0. Heated-bed capabilities are unchanged, so bed temperature can be set.

3. Relative extrusion distances must be used because of the feed system program logic, which adds each extrusion length.

4. Filament diameter must be set to the value used in the stepping factor calculation from Eq. 3. A diameter of 3 mm works well according to the auger geometry. Slic3r uses this diameter setting in combination with the E_steps value (found in the configuration tab of the Taz 6's liquid crystal display [LCD] screen) to calculate the volume of plastic filament fed into the heating chamber per stepper motor revolution. The E_steps value stores the number of stepper motor steps to move the plastic filament 1 mm. Taz 6 firmware executes stepping in sixteenth-step mode, which results in a total of 3200 steps per revolution for the 1.8° NEMA 17 stepper motor. To calculate the filament diameter setting for Slic3r, the volume of material extruded per revolution for the specific auger must be known. The calculation is done with Eq. 6.

$$D_F = \sqrt{\frac{V_A * E\_steps}{800 * \pi}}, \tag{6}$$

   where DF is filament diameter, VA is auger extrusion volume per revolution, and E_steps is the configuration value set through the Taz 6's LCD screen.

5. Lulzbot Taz 6 printers use a 'safe homing position' for z-homing, which enables the z-stop limit switch to home the nozzle-tip position instead of an arbitrary end-stop switch position.

6. The custom start, stop, and toolhead change G-code must be pasted into the Printer Settings > Custom G-code Slic3r profile section. The toolhead change G-code moves the print head to the dumping location, far right of bed, purges an extrusion length of 400 mm, pauses to let the user wipe off the nozzle, and then resumes printing.

Custom Start G-code:

;This G-Code has been generated specifically for the LulzBot TAZ 6 with Custom DIW print head
M73 P0 ; clear GLCD progress bar
M75 ; start GLCD timer
G26 ; clear potential 'probe fail' condition
M107 ; disable fans
M420 S0 ; disable previous leveling matrix
G90 ; absolute positioning
M82 ; set extruder to absolute mode
G92 E0 ; set extruder position to 0
G28 ; Home all axis
G1 E-10 F100 ; retract filament
G1 X-9 Y-9 F3000 ; move above first probe point
M204 S100 ; set probing acceleration
G29 ; start auto-leveling sequence
M420 S1 ; activate bed level matrix
M425 Z ; use measured Z backlash for compensation
M425 Z F0 ; turn off measured Z backlash compensation.
G1 X0 Y0 Z15 F5000 ; move up off last probe point
G4 S1 ; pause
M400 ; wait for moves to finish
G1 Z2 E10 F75 ; prime tiny bit of filament into the nozzle
M117 DIW System Printing… ; progress indicator message on LCD

Custom Stop G-code:

M400 ; wait for moves to finish
M107 ; disable fans
G91 ; relative positioning
G1 E-1 F300 R-1.00 ; filament retraction to release pressure
G1 Z2 E-5 X-20 Y-20 F3000 ; lift up and retract even more filament
G90 ; absolute positioning
G1 X206 Y236 F3000
G1 Z3 F600
M77 ; stop GLCD timer
M84 ; disable steppers
M117 Print Complete. ; print complete message

Custom Tool-head Switch G-code:

; Change T0,T1 to R0,R1 and move it directly above this line at the end of the most recent G1 line.
G1 F1500 X295 Y115 ; Purge Gcode
G4 S5
G1 F100 E50
G1 F100 E50
G1 F100 E50
G1 F100 E50
G1 F100 E50
G1 F100 E50
G1 F100 E50
G1 F100 E50
G4 S15

Once a part has been sliced and the G-code has been generated, ratio commands must be manually entered into the G-code file using a text editor. Add a ratio command to the end of the first G1 line after the custom start G-code. Then, add ratio commands at other desired locations to change the ratio during the print. For example, if the user wants to start with 100% material A, R0.00 would be entered. Then, if the user wants to change to a ratio of 50% material A and 50% material B, R0.50 would be entered. And finally, to switch to 100% material B, R1.00 would be entered. Alternatively, if binary material switches are desired, multimaterial settings in Slic3r can be used to automatically add the toolhead change G-code followed by "T0" or "T1" for toolhead 1 or 2. The T can be changed to R using a text editor and moved to the G1 line directly above the custom toolhead switch G-code. The ratio command must be placed at the end of a G1 line, because if it is placed on a separate line it will be ignored and will not be echoed to the feed system microcontroller.

3. Results and Discussion

Damage tolerance is highly dependent on sintered density because even small imperfections will induce stress concentrations that lead to failure. A prerequisite of high sintered density is high green density, which requires an optimized printing process. An optimized printing process should reduce air bubbles, defects, warping, and slumping. Several areas of the printing process must be optimized including ink rheology, auger geometry, and G-code generation. Rheology will be optimized to increase ink printability. The auger geometry will be optimized with a focus on

the mixing–dead space relationship and reduction of air bubbles. The G-code design workflow will be optimized using a print complexity timeline.

The highly loaded, colloidal ceramic inks used for DIW contain around 50 vol.% ceramic powder, 5 vol.% binder, 5 vol.% dispersant, and water. To produce inks with yield-pseudoplastic behavior, each ceramic powder type must be characterized for surface chemistry, particle size, and shape. This information can then be used to choose a specific binder/dispersant system that will effectively disperse the colloids, while providing adequate green body strength. Correct rheology is critical for printed parts to retain their shape, while still allowing extrusion through a fine tip. In-line mixing and dead space, which is the volume of material in the nozzle between the ink inlets and tip, must be optimized to enable development of complex, heterogeneous structures. Mixing facilitates the development of gradient structures with smooth, controllable compositional changes, while reducing dead space allows for quick compositional changes. Figure 10 illustrates a feasible mechanism for in-line mixing. The difference in interaction between the ceramic ink and barrel wall versus auger surface drives mixing convection cells. If particles show a stronger interaction with the barrel wall than the auger surface, the convection cells will be driven in the directions shown in Fig. 10. Adequate mixing can be achieved using a long auger screw, but a long screw will result in a large dead space. These competing factors must be balanced to allow both rapid changes in composition and sufficient mixing.

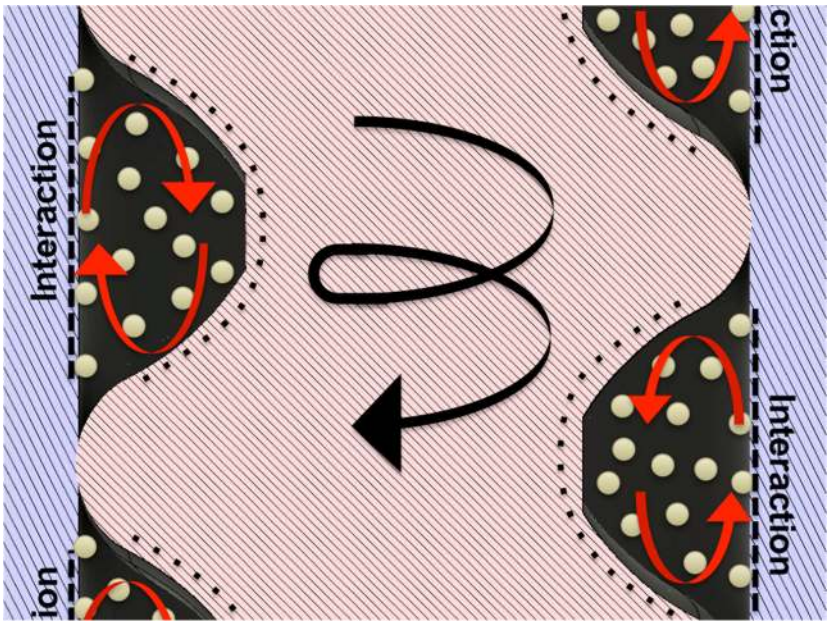

Fig. 10 In-line mixing diagram showing mixing convection cells driven by particle interaction with the barrel (purple) and auger (pink) during auger rotation

Following the development of optimized inks and auger geometry, printing parameters are fine-tuned for each print. The capability to print with multiple materials and mix in-line enables both discrete layers and gradients of composition. Relevant parameters include raster speed, trace width and height, layer change settings, and feature sequence (walls versus infill first). Radial gradients can be formed by priming material A, starting the infill in the center, and switching to 100% material B immediately. Due to the dead space, the composition change will occur over a number of traces. Figure 11 shows a radial gradient printed using two colors of Play-Doh. The switch from blue to white takes the majority of the shown layer, with only the last four perimeters at 100% white Play-Doh. Figure 12 shows a layer-wise gradient of boron carbide to silicon carbide, where the composition was changed by 10% each layer. Figure 13 shows a layered boron carbide and silicon carbide print, with an ABAB pattern. A G-code error resulted in the second layer remaining material A. Prime and purge steps are used to create layered parts. As an A layer finishes, material B is primed, material A is reversed, the dead space is purged into a dumping container, and then the next layer is started. DIW process optimization will drive the advancement and capability of this system; successful optimization will result in the printing of heterogeneously graded parts with structural organization at multiple length-scales.

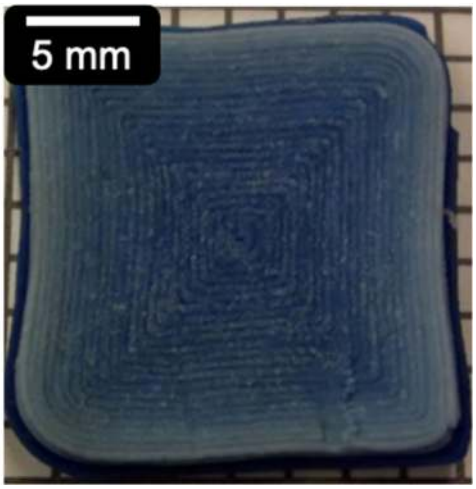

Fig. 11 Radial gradient printed using blue and white Play-Doh. Print parameters are 0.6-mm layer height, 0.8-mm nozzle width, 10-mm/s print head speed, and center-to-perimeter concentric fill pattern.

Fig. 12 Gradient boron carbide (bottom) to silicon carbide (top) 1-inch diameter cylinder produced by DIW. Print parameters are 1.2-mm layer height, 1.2-mm nozzle width, 4-mm/s print head speed, and center-to-perimeter concentric fill pattern.

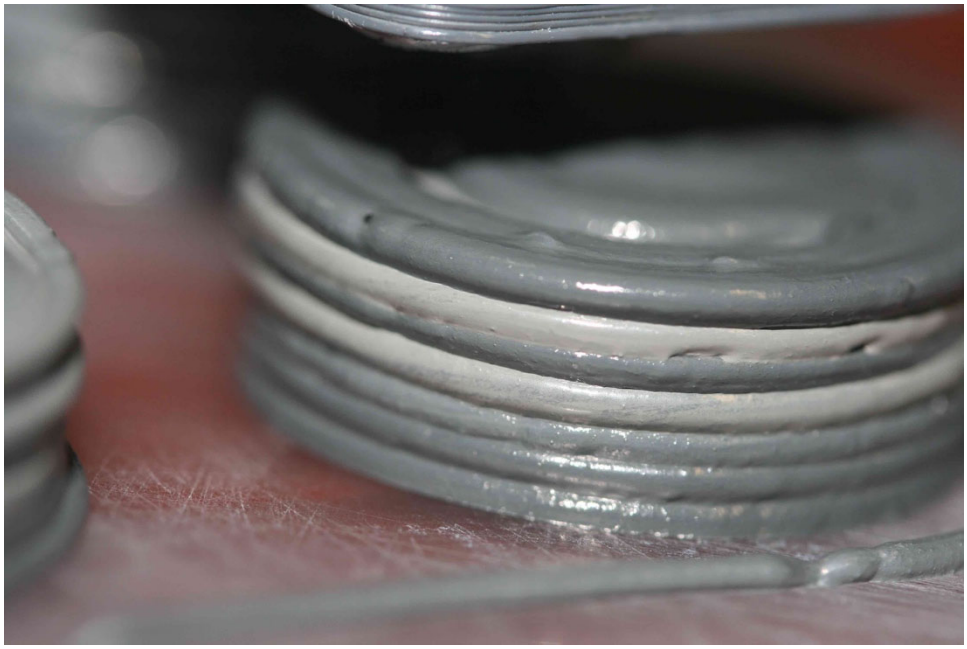

Fig. 13 Layered boron carbide (dark-gray) and silicon carbide (light-gray) 1-inch diameter cylinder produced by DIW. Print parameters are 1.2-mm layer height, 1.2-mm nozzle width, 4-mm/s print head speed, and center-to-perimeter concentric fill pattern.

This custom DIW system, shown in Fig. 14, addresses several deficiencies many other ceramic AM platforms have, including those of other DIW systems. AM systems that can print with multiple materials throughout a single print are limited to extrusion-based systems, due to the difficulty of switching material types when using a powder or liquid bed. Commercially available DIW systems tend to use a plunger to extrude material from a syringe. Plunger-driven extrusion systems require a tool head switch to change composition and cannot print composition gradients. These deficiencies reduce their ability to print functional structures and take advantage of extrinsic toughening mechanisms.

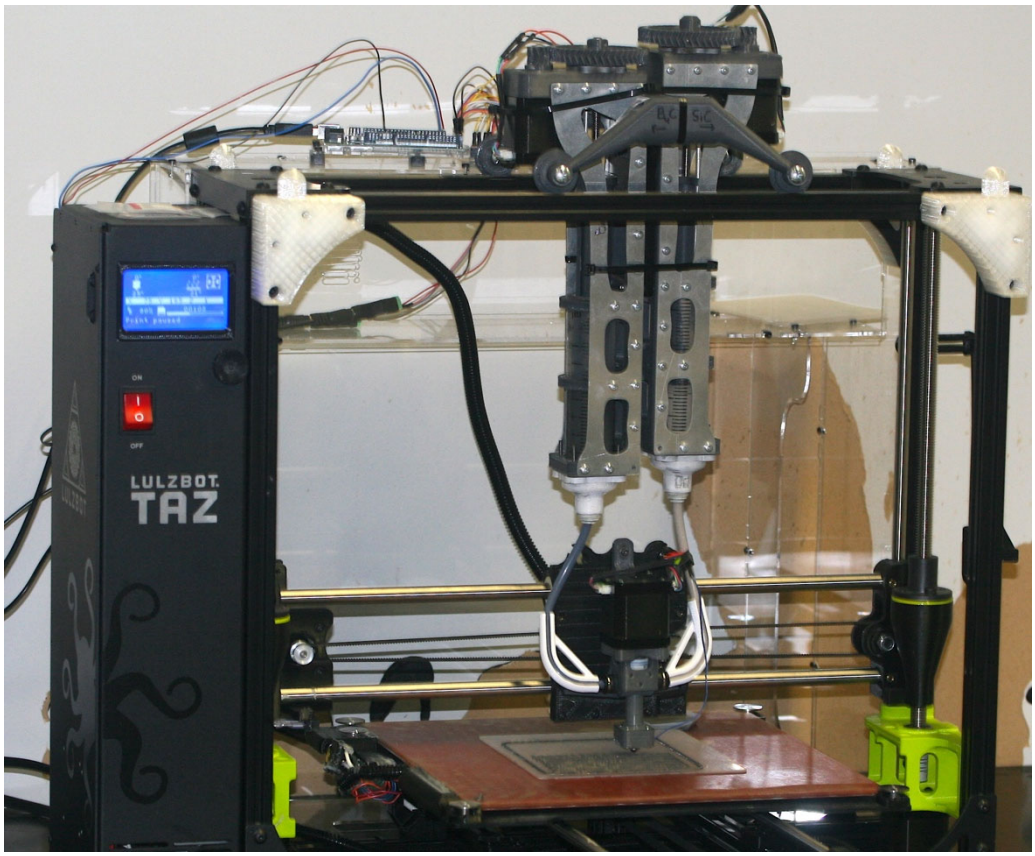

Fig. 14 Custom DIW system mounted on a Lulzbot Taz 6 printer. A rolling truss allows the feed system to follow the x-axis motion of the print head. This system has multimaterial and in-line mixing capabilities, which enable printing of functionally graded ceramic composites.

4. Conclusions

This report summarizes the development of a custom DIW system with multimaterial and in-line mixing capabilities for use with yield-pseudoplastic ceramic inks. The DIW system gives researchers the means to study the effects of functional design on ballistic performance in composite ceramic armor. Additionally, models of the structure-property relationship can be developed and

verified for dynamic responses in composite ceramics. Finally, armor designs inspired from notably tough biological structures including fish scales and abalone nacre can be tested.

Future work includes additional optimization of the auger, modification of the print head barrel to allow heating to adjust ink viscosity, modification of the print head nozzle to allow polarization of magnetically susceptible inks, and the addition of a UV light to allow printing of UV curable inks.

5. References

1. Carter CB, Norton G. Ceramic materials: science and engineering, 1st ed. New York (NY): Springer; 2007.

2. Yang W, Gludovatz B, Zimmermann EA, Bale HA, Ritchie RO, Meyers MA. Structure and fracture resistance of alligator gar (*Atractosteus spatula*) armored fish scales. Acta Biomater. 2013;9(4):5876–5889.

3. Meyers MA, Lin AYM, Chen PY, Muyco J. Mechanical strength of abalone nacre: role of the soft organic layer. J Mech Behav Biomed Mater. 2008;1(1):76–85.

4. Sherman VR, Quan H, Yang W, Ritchie RO, Meyers MA. A comparative study of piscine defense: the scales of *Arapaima gigas*, *Latimeria chalumnae* and *Atractosteus spatula*. J Mech Behav Biomed Mater. 2017;73:1–16.

5. Franks GV, Tallon C, Studart AR, Sesso ML, Leo S. Colloidal processing: enabling complex shaped ceramics with unique multiscale structures. J Am Ceram Soc. 2017;100(2):458–490.

6. Lewis JA. Colloidal processing of ceramics. J Am Ceram Soc. 2004;83(10):2341–2359.

7. Vargas-Gonzalez L, Speyer RF, Campbell J. Flexural strength, fracture toughness, and hardness of silicon carbide and boron carbide armor ceramics. Int J App. Ceram Technol. 2010;7(5):643–651.

8. Malmal Moshtaghioun B, Ortiz AL, Gómez-García D, Domínguez-Rodríguez A. Toughening of super-hard ultra-fine grained B4C densified by spark-plasma sintering via SiC addition. J Eur Ceram Soc. 2013;33(8):1395–1401.

9. Launey ME, Ritchie RO. On the fracture toughness of advanced materials. Adv Mater. 2009; 21(20):2103–2110.

10. Lange FF. Powder processing science and technology for increased reliability. J Am Ceram Soc. 1989;72(1):3–15.

List of Symbols, Abbreviations, and Acronyms

2-D, 3-D	two-dimensional, three-dimensional
ABS	acrylonitrile butadiene styrene
AM	additive manufacturing
BED	Big Easy Driver
CAD	computer-aided design
DIW	direct ink writing
FDM	fused deposition modeling
LCD	liquid crystal display
PTC	push-to-connect
SD	secure digital
UV	ultraviolet

1 (PDF) DEFENSE TECHNICAL INFORMATION CTR DTIC OCA

1 (PDF) CCDC ARL FCDD RLD CL TECH LIB

24 (PDF) CCDC ARL FCDD RLD H MAUPIN M TSCHOPP P KHOOSHABEHADEH FCDD RLW J ZABINSKI A RAWLETT FCDD RLW B C HOPPEL L VARGAS-GONZALEZ R BECKER P GILLICH A TONGE B SCHUSTER J CAMPBELL FCDD RLW D E ROBINETTE FCDD RLW M B LOVE J LA SCALA FCDD RLW MD K CHO M PEPI J YU FCDD RLW ME S SILTON J LASALVIA J PELZ N KU FCDD RLW MG N ZANDER FCDD RLS RE H TSANG